EarthArXiv coversheet for:

Title: (Full title) Friction law for earthquake nucleation: size doesn't matter

Authors

Yuntao Ji[1,3*], André R. Niemeijer[1], Dawin H. Baden[1], Futoshi Yamashita[2], Shiqing Xu[2,4], Luuk B. Hunfeld[1,6], Ronald P. J. Pijnenburg[1], Eiichi Fukuyama[2,5], Christopher J. Spiers[1]

Affiliations

[1]HPT Laboratory, Faculty of Geosciences, Utrecht University; Utrecht, 3584 CB, the Netherlands.

[2]National Research Institute for Earth Science and Disaster Resilience; Tsukuba, 305-0006, Japan.

[3]State Key Laboratory of Earthquake Dynamics, Institute of Geology, China Earthquake Administration; Beijing, 100029, China.

[4]Department of Earth and Space Sciences, Southern University of Science and Technology; Shenzhen, 518055, China.

[5]Department of Civil and Earth Resources Engineering, Kyoto University; Kyoto, 615-8530, Japan.

[6]Advisory Group for Economic Affairs, the Netherlands Organization for Applied Scientific Research (TNO), Energy Transition Unit; Utrecht, 3584 CB, the Netherlands

*Corresponding author. Email: y.ji@uu.nl

Statement

Title

- (Full title) Friction law for earthquake nucleation: size doesn't matter
- (Short title) Upscaling fault friction: Size doesn't matter

Authors

Yuntao Ji[1,3*], André R. Niemeijer[1], Dawin H. Baden[1], Futoshi Yamashita[2], Shiqing Xu[2,4], Luuk B. Hunfeld[1,6], Ronald P. J. Pijnenburg[1], Eiichi Fukuyama[2,5], Christopher J. Spiers[1]

Affiliations

[1]HPT Laboratory, Faculty of Geosciences, Utrecht University; Utrecht, 3584 CB, the Netherlands.

[2]National Research Institute for Earth Science and Disaster Resilience; Tsukuba, 305-0006, Japan.

[3]State Key Laboratory of Earthquake Dynamics, Institute of Geology, China Earthquake Administration; Beijing, 100029, China.

[4]Department of Earth and Space Sciences, Southern University of Science and Technology; Shenzhen, 518055, China.

[5]Department of Civil and Earth Resources Engineering, Kyoto University; Kyoto, 615-8530, Japan.

[6]Advisory Group for Economic Affairs, the Netherlands Organization for Applied Scientific Research (TNO), Energy Transition Unit; Utrecht, 3584 CB, the Netherlands

*Corresponding author(s)

Email: y.ji@uu.nl

Abstract

The nucleation phase is key to earthquake forecast. A central question in modeling earthquake nucleation is whether fault frictional properties measured in the laboratory are applicable to nature. However, it is unknown whether laboratory fault friction data are even suitable for the mesh size (~1m) of the seismic simulator used in the seismic hazard analysis. We report the first meter-scale frictional sliding experiments performed on simulated frictional wear material (fault gouge). The results show that macroscopic fault friction and its dependence on slip rate, slip distance and gouge state are indistinguishable from those measured at the cm scale, despite major spatial heterogeneities in stress and slip velocity. We attribute this scale independence to slip being accommodated on microscale shear bands in experiments at all scales. The implication is that parameters derived from conventional friction experiments are directly applicable to modelling induced and natural earthquake rupture nucleation at current mesh resolution.

Teaser

Fault sliding experiments show scale-independent friction despite spatial heterogeneity in stress and slip distribution.

MAIN TEXT (*maximum of 15,000 words*)

Introduction

Human activities in the sub-surface are increasing steadily due to growing demand for resources ranging from natural gas and geothermal energy to geological storage capacity for CO_2 or green hydrogen. One risk in exploiting such resources is induced seismicity caused by reactivation of pre-existing faults. A prime example is seen in the Groningen gas field (Netherlands), one of the world's largest onshore fields. Seismic events caused by gas production have been recorded here since 1991, the largest being the 2012 M_L3.6 Huizinge earthquake, which generated considerable public unrest (*1*), leading to a government decision to advance field closure from ~2040 to 2022. Other examples include the many earthquakes recently recorded in Oklahoma, due to waste water injection, and the 2006 M_L 3.4 Basel and 2017 Mw 5.5 Pohang events related to geothermal reservoir stimulation (*2*)(*3*)(*4*).

To evaluate the hazard associated with both induced and natural seismicity (*5*), physics-based numerical models that address rupture nucleation and propagation on faults are key(*6*)(*7*). The Rate-and-State dependent Friction (RSF) equations are widely used in modelling earthquake rupture nucleation(*8*)(*9*)(*10*) and assessing hazard (*11*) . These empirical equations are derived from cm-scale laboratory experiments on site-relevant fault rocks, and capture the frictional response of the fault dynamic system due to a step change in loading conditions. However, this approach neglects potential length-scale effects associated with natural variations in fault zone topography, thickness, internal structure and composition (*12*). Heterogeneities are inevitable in laboratory experiments too, due to the finite boundary conditions, nonuniformly imposed stress and localization of deformation. To date, it remains unknown whether a simulated fault at the cm-scale captures behaviour at the m-scale, which is the smallest mesh resolution that is currently feasible in numerical earthquake simulators. While several numerical and field studies have considered how fault roughness and other mechanical irregularities may lead to length-scaling of fault mechanical behaviour (*13*)(*14*), experimental validation at the appropriate length scale is lacking, even for the simplest case of a homogeneous laboratory fault with no deliberately imposed heterogeneities.

Results

Friction properties

We report 18 large-scale friction experiments on simulated sandstone fault gouge, sandwiched between 2 m sandstone slider-blocks. The gouge layers measured 0.5, 1.0 or 1.5 m in length by 10 cm wide and 1-5 mm initial (unloaded) thickness. The experiments were performed on room-dry gouge using the large biaxial (shaking-table) machine(*15*), operated in constant-velocity and stepped-velocity modes (0.01-0.1-1.0 mm/s) and employing normal stresses of 1.5 – 9.0 MPa. We used crushed sandstone from the Groningen reservoir as gouge material and a similar (Agra) sandstone as slider blocks. Deformation and displacement of the blocks were measured on opposite sides of the assembly using i) regularly spaced strain gauges, located 2 cm below the gouge layer, and ii) high-resolution digital image correlation (DIC) involving a speckled marker-pattern and high-speed digital photography (see Supplement). We test whether the measured macroscopic frictional properties are scale-dependent by comparing the results with data obtained in 8 experiments performed on the same, room-dry gouge at the 5 and 21 cm scales.

To describe the quasi-static frictional properties measured at all scales, we use standard RSF laws (*16*)(*17*):

$$\mu = \mu_0 + a \ln \frac{V}{V_0} + b \ln \frac{V_0 \theta}{d_c} \qquad (1)$$

$$\frac{d\theta}{dt} = -\frac{V\theta}{d_c} \ln \frac{V\theta}{d_c} \qquad (2)$$

Here, μ is the friction coefficient (shear-stress / normal-stress), a, b and $(a-b)$ describe the rate and state dependence of fault friction, and d_c is the critical slip distance over which friction evolves towards a new steady state upon a change in load-point velocity. Equation 2 (the Ruina slip evolution law (*18*)) provided the best description of internal fault state θ and its evolution $d\theta/dt$. We performed non-linear least-square inversions using Eq.1 and Eq.2, coupled with an equation describing the elastic interaction of the sample and loading frame, to obtain a, b and d_c over 2-43 velocity-steps performed per experiment (table S1).

Our large-scale experiments exhibited friction coefficients of 0.66~0.69, similar to conventional cm/dm-scale tests. The results for $(a-b)$ and d_c at the m-scale are shown in Figure 1 (green triangles), omitting data obtained in velocity steps to 1 mm/s because of finite acceleration which conflicts with the assumption of an instantaneous velocity change in RSF fitting (see Supplement). In addition, Figure 1 shows data from our 8 experiments performed at the 5 cm (Rome) and 21 cm (Utrecht) scales, plus literature data (*19*) on room-dry quartz gouge at the 5 cm scale. All $(a-b)$ and d_c data fall within the same range and follow a similar trend, regardless of experimental length scale. A gentle decrease in $(a-b)$ and d_c with increasing slip distance or gouge shear strain γ, is visible at $\gamma<10$ (see also (*19*)), with $(a-b)$ becoming negative (potentially unstable, velocity-weakening slip) at $\gamma>10$.

Spatio-temporal heterogeneity

Aside from the d_c data of Marone and Kilgore(*19*), which was obtained at high normal stresses (25 MPa) known to reduce d_c (*20*), the above RSF analysis shows no distinguishable scale effect between meter- and centimeter-scale samples, and no effect of gouge layer thickness. Since scale effects, notably on d_c, are generally expected to be associated with spatial heterogeneities in stress (asperities) on the fault plane(*13*)(*21*), our RSF data suggest that little such heterogeneity exists, even within our 0.5-1.5 m experiments. However, these experiments in fact exhibited major heterogeneities in stress, displacement and strain in and around the gouge layer, during initial normal loading and during sliding. Specifically, pressure-sensitive-sheets, placed on each gouge layer to record initial normal loading and then removed prior to reloading and shear, showed order-of-magnitude variations in normal stress (Fig. 2, A to C). Normal stresses upon reloading, calculated from the strain gauges on the lower block plus the sandstone's elastic constants, show a close match with the pressure-sensitive-sheet data (Fig. 2, C and D; $\sigma_n = \sigma_{yy}$), confirming the heterogeneity and demonstrating that the strain gauges provide a good estimate of stresses acting on the gouge layer.

Before and in the earliest stages of all shearing experiments at the 0.5-1.5 m scale ($\gamma<2$: dotted red lines in Fig.2, C and D, darkest brown lines and dots in Fig.2, D to F), normal stresses $\sigma_n = \sigma_{yy}$ are high at the ends of the gouge layer but low in the center. As shearing progresses (colored curves in D and E), shear stress $\tau = \sigma_{xy}$ remains low at the west and high at the east ends of the gouge layer, while normal stress becomes more uniform. This is seen in all faults investigated (fig.S12).

In addition to these heterogeneities in normal and shear stress, which frequently reach a factor 10, we examined the spatial and temporal distribution of i) relative velocity (shear and normal components) measured block-to-block directly across the gouge layer, and ii) stress within the confining sandstone blocks, during individual steps in applied or "load point" velocity. Local velocities were obtained using the displacements and velocities calculated from the digital imaging and DIC methods described above; stresses were computed from the strain gauge data (see Supplement). We show the processed DIC and stress results obtained during and after a representative velocity up-step in Fig. 3, B to

G. The associated macroscopic friction response is shown in Fig. 3A. Load point velocity was changed from 0.01 to 0.1 mm/s at time t=219.8 s, producing an increase in friction coefficient towards a peak value (the direct effect, magnitude $a.ln\ (V/V_0)$) at t=220.16 s, followed by a decrease to a minimum value at t = 220.4 s and a final "rebound" (attenuated oscillation) to a new steady value at t = 221.7 s (evolution effect $b.ln(V/V_0)$). The strain-gauge- and DIC-derived data (Fig. 3, B and C, D to G) correspond to the time window covering the direct effect (t=219.8 s – 220.16 s) and the subsequent friction drop (t=220.16 s – 220.4 s). Fig. 3, B to C displays the shear stress distribution along the fault, and its evolution with time, for the duration of the direct effect plus friction drop. Here, the shear stress evolution $\Delta\tau$ is the change measured relative to the initial stress at the beginning of the corresponding time interval. Fig. 3, D to E shows the across-fault shear velocity (expressed as the departure from the average shear velocity taken over all measurement points along the fault at any instant) and how this evolves along the fault with time. In this way, we establish where and when slip starts to accelerate as the load point velocity is changed. In Fig. 3, F to G, we plot the across-fault dilation velocity normal to the gouge layer at every measurement location, to extract variations in vertical dilation(+)/compaction(-) rate with position and time.

These data demonstrate a marked shear stress concentration or asperity at horizontal position $1200 \leq x \leq 1500$ mm (Fig.2, D and E; Fig.3, B and C). During the macroscopic direct effect stage (Stage I, Fig.3A), slip velocities start to diverge in that the low-stress region ($500 \leq x \leq 900$ mm) slips faster than the asperity region (Fig. 3D), where right-lateral(+) shear stress accumulates (Fig. 3B). Upon entering the stress drop stage (Stage 2), slip in the asperity region accelerates rendering it the fastest slipping segment (Fig.3E), while shear stress drops by~0.2 MPa. At the same time, the asperity dilates, while the low-stress region compacts (Fig.3G). During both stages, the asperity is responsible for most relative stress accumulation and subsequent release (Fig. 3, B and C). Our analysis thus shows that the acceleration accompanying a macroscopic velocity up-step initiates in low-stress regions and then transfer to high-stress asperities, instead of occurring simultaneously and uniformly over the gouge layer. In other words, fault slip velocity, dilation and stress all show substantial spatial variation upon a macroscopic change in driving velocity, and yet the associated macroscopic RSF parameters obtained at m-scale are indistinguishable from data obtained in experiments at the cm-dm scale (Fig.1), i.e. there are no detectable length scale effects.

Discussion

We suggest that this result emerges because fault motion is accommodated by slip on self-organizing, micrometer-wide shear bands, spaced on the mm scale, which we observe throughout the gouge in our m-scale and cm/dm-scale experiments (Fig. 4). Previous gouge experiments at the cm-scale (*20*) show identical slip-localization features, with (a-b) being insensitive to normal stress, while d_c decreases slightly as normal stress increases. We propose that the scale-independence of RSF parameters seen in our cm-m scale gouge experiments occurs because these parameters are largely insensitive to normal stress, and hence to normal stress heterogeneities, and because slip is accommodated on microscale shear bands with self-organizing mm spacing and internal grain size and structure (*cf. 16*) that evolve in the same way at all experiment scales. This is supported by the trend in RSF parameters with increasing shear strain illustrated in Fig. 1. The implication is that fault size does not affect the governing gouge friction law during earthquake rupture nucleation, at least up to length scales of 1-2 m, which is the mesh scale used in state-of-the-art models addressing induced and natural seismicity.

Materials and Methods

Overview of all experiments performed

The main body of experiments reported in this paper consists of 18 large-scale friction experiments performed on simulated sandstone fault gouge layers, sandwiched between two sandstone slider-blocks. The upper sandstone block was 1.5m long, and the lower block was 2m long. The gouge layers measured 0.5, 1.0 or 1.5 m in length, by 10 cm in width and 1-5 mm initial thickness. The experiments were performed on room-dry gouge in direct shear mode, and at ambient temperature, using the large biaxial (shaking table) machine at The National Research Institute for Earth Science and Disaster Resilience (NIED, Tsukuba, Japan (*15*)(*23*)(*24*)). In addition, we performed smaller scale friction experiments on the same gouge, and under the same conditions, using the room-temperature, rotary-shear testing machine at Utrecht University (length scale ~21 cm – described by (*25*)) as well as the double-direct shear machine at La Sapienza University, Rome (length scale 5 cm – described by (*26*)(*27*)). All experiments reported are listed below, along with the corresponding sample dimensions, apparatus and experimental conditions - see Table S1. We focus here on describing the large-scale experiments conducted at NIED. The apparatus, experimental approach and data reduction methods employed in the experiments performed at Utrecht and Rome were more conventional in nature - see above-mentioned references.

Large-scale experimental apparatus

The large-scale friction apparatus used in the present study is the second generation version of the large biaxial (shaking table) machine at NIED (*15*)(*23*) – see Fig. S1. In this direct shear machine, shear displacement and hence shear force is applied to the experimental fault by means of relative motion established between the moving shaking table, which carries the experimental fault assembly, and the stationary concrete floor surrounding the shaking table. A metal arm or reaction force bar connects the upper sandstone forcing block of the shear assembly to the concrete floor via a support frame (Fig. S1), so that the upper block is held stationary relative to the shaking table. Thus, aside from small elastic strains within the loading system, the upper block is fixed to and in effect pushed by the reaction bar, relative to the lower sandstone block, which is rigidly fixed to the shaking table by stiff steel supports that are bolted to the shaking table. Three hydraulic jacks impose vertical normal load on the upper and lower rock forcing blocks, via an enveloping loading frame (Fig. S1). A 1.5 m-long steel plate, located between the jacks and upper rock forcing block, helps ensure a uniform normal stress over the full top surface of the upper rock block. A roller system located between the three jacks and the upper bar of the normal loading frame (Fig. S1) ensures that relative motion is free to occur in the horizontal (x-) direction, enabling large shear displacements to be applied to the experimental fault between the two rock forcing blocks, while simultaneously applying normal stress.

Sandstone forcing blocks and gouge material

We conducted our large-scale direct shear experiment using a pair of forcing blocks made of Agra sandstone extracted from a quarry in India and supplied to NIED in final machined form (Fig. S2) by Sekistone Co. Ltd., Gifu, Japan. The lower block is a cuboid of dimensions 2 m × 0.5 m × 0.1 m in the x, y, and z directions as defined in Fig. S2 (see also Fig. S1). The upper block is a cuboid with a central, square-sectioned ridge pointing downwards, which rests lengthwise on the lower block to form the (gouge-filled)

experimental fault. The dimensions of the cuboidal trunk of the upper block are 1.5 m × 0.4 m × 0.5 m in the x, y, z directions, while the central ridge located on the bottom surface has dimension of 1.5 m × 0.1 m × 0.1 m (length × height × width) in these directions (see Fig. S2). Thus, the width of the experimental fault surface, i.e. of the gouge layer used in the present experiments, is 0.1 m and the length is up to 1.5 m.
The sandstone forcing blocks were prepared in the above dimensions by Sekistone. The company ground the fault plane surfaces (i.e., the top surface of the lower block and the bottom surface of the upper block) with an 8-m-long surface grinder, finishing with #60 grade SiC grit. The roughness R_a of the finished sandstone surfaces was measured using a profilometer and shown to lie in the range 15.5 μm to 19.5 μm.

The properties of Agra sandstone were measured at the HPT laboratory at Utrecht using an Instron uniaxial load frame to obtain quasi-static elastic constants and the Archimedes method to measure sample density. The results yielded Poisson's ratio ν = 0.16, Young's modulus E = 20.51 GPa, Shear modulus G = 8.84 GPa, and density ρ = 2.257g/cm^3.

Gouge material was prepared from Slochteren sandstone core obtained from the Groningen gas field by the field operator, NAM (https://www.nam.nl/english-information.html). The grain size distribution ranges from 0.1 μm to 300 μm, with a major peak at about 55 μm and a minor peak at around 1μm. Before each experiment, we spread the gouge on the lower block's top surface as evenly as possible, using a coarse sieve plus aluminum templates to fix gouge-layer dimensions and initially applied thicknesses (1, 2, 3, 4, and 5 mm).

References

1. N. Van der Voort, F. Vanclay, Social impacts of earthquakes caused by gas extraction in the Province of Groningen, The Netherlands. *Environ. Impact Assess. Rev.* **50**, 1–15 (2015).
2. N. Deichmann, D. Giardini, Earthquakes induced by the stimulation of an enhanced geothermal system below Basel (Switzerland). *Seismol. Res. Lett.* **80**, 784–798 (2009).
3. K.-H. Kim, J.-H. Ree, Y. Kim, S. Kim, S. Y. Kang, W. Seo, Assessing whether the 2017 Mw 5.4 Pohang earthquake in South Korea was an induced event. *Science (80-.).* **360**, 1007–1009 (2018).
4. F. Grigoli, S. Cesca, A. P. Rinaldi, A. Manconi, J. A. López-Comino, J. F. Clinton, R. Westaway, C. Cauzzi, T. Dahm, S. Wiemer, The November 2017 Mw 5.5 Pohang earthquake: A possible case of induced seismicity in South Korea. *Science (80-.).* **360**, 1003–1006 (2018).
5. S. Barbot, N. Lapusta, J. Avouac, Under the hood of the earthquake machine: Toward predictive modeling of the seismic cycle. *Science (80-.).* **336**, 707–710 (2012).
6. N. Lapusta, J. R. Rice, Y. Ben‐Zion, G. Zheng, Elastodynamic analysis for slow tectonic loading with spontaneous rupture episodes on faults with rate‐ and state‐dependent friction. *J. Geophys. Res. Solid Earth*. **105**, 23765–23789 (2000).
7. L. Buijze, P. A. J. van den Bogert, B. B. T. Wassing, B. Orlic, Nucleation and Arrest of Dynamic Rupture Induced by Reservoir Depletion. *J. Geophys. Res. Solid Earth*. **124**, 3620–3645 (2019).
8. J. H. Dieterich, Earthquake nucleation on faults with rate-and state-dependent strength. *Tectonophysics*. **211**, 115–134 (1992).
9. A. M. Rubin, J. Ampuero, Earthquake nucleation on (aging) rate and state faults. *J.*

Geophys. Res. Solid Earth. **110** (2005).

10. J. Ampuero, A. M. Rubin, Earthquake nucleation on rate and state faults–Aging and slip laws. *J. Geophys. Res. Solid Earth*. **113** (2008).
11. B. E. Shaw, K. R. Milner, E. H. Field, K. Richards-Dinger, J. J. Gilchrist, J. H. Dieterich, T. H. Jordan, A physics-based earthquake simulator replicates seismic hazard statistics across California. *Sci. Adv.* **4**, 1–10 (2018).
12. D. R. Faulkner, C. A. L. Jackson, R. J. Lunn, R. W. Schlische, Z. K. Shipton, C. A. J. Wibberley, M. O. Withjack, A review of recent developments concerning the structure, mechanics and fluid flow properties of fault zones. *J. Struct. Geol.* **32**, 1557–1575 (2010).
13. Y. Tal, B. H. Hager, J. P. Ampuero, The effects of fault roughness on the earthquake nucleation process. *J. Geophys. Res. Solid Earth*. **123**, 437–456 (2018).
14. T. Candela, E. E. Brodsky, The minimum scale of grooving on faults. *Geology*. **44**, 603–606 (2016).
15. E. Fukuyama, K. Mizoguchi, F. Yamashita, T. Togo, H. Kawakata, N. Yoshimitsu, T. Shimamoto, T. Mikoshiba, M. Sato, C. Minowa, Large-scale biaxial friction experiments using a NIED large-scale shaking table. *Rep Nat'l Res Inst Earth Sci Disas Prev*. **81**, 15–35 (2014).
16. J. H. Dieterich, Modeling of rock friction: 1. Experimental results and constitutive equations. *J. Geophys. Res. Solid Earth*. **84**, 2161–2168 (1979).
17. A. Ruina, Slip instability and state variable friction laws. *J. Geophys. Res. Solid Earth*. **88**, 10359–10370 (1983).
18. C. Marone, Laboratory-derived friction laws and their application to seismic faulting. *Annu. Rev. Earth Planet. Sci.* **26**, 643–696 (1998).
19. C. Marone, B. Kilgore, Scaling of the critical slip distance for seismic faulting with shear strain in fault zones. *Nature*. **362**, 618–621 (1993).
20. M. M. Scuderi, C. Collettini, C. Viti, E. Tinti, C. Marone, Evolution of shear fabric in granular fault gouge from stable sliding to stick slip and implications for fault slip mode. *Geology*. **45**, 731–734 (2017).
21. G. Hillers, Y. Ben‐Zion, P. M. Mai, Seismicity on a fault controlled by rate‐ and state‐dependent friction with spatial variations of the critical slip distance. *J. Geophys. Res. Solid Earth*. **111** (2006).
22. J. S. Tchalenko, Similarities between shear zones of different magnitudes. *Geol. Soc. Am. Bull.* **81**, 1625–1640 (1970).
23. T. Togo, T. Shimamoto, F. Yamashita, E. Fukuyama, K. Mizoguchi, Y. Urata, Stick–slip behavior of Indian gabbro as studied using a NIED large-scale biaxial friction apparatus. *Earthq. Sci.* **28**, 97–118 (2015).
24. F. Yamashita, E. Fukuyama, S. Xu, K. Mizoguchi, H. Kawakata, S. Takizawa, Rupture preparation process controlled by surface roughness on meter-scale laboratory fault. *Tectonophysics*. **733**, 193–208 (2018).
25. P. Kumar, E. Korkolis, R. Benzi, D. Denisov, A. Niemeijer, P. Schall, F. Toschi, J. Trampert, On interevent time distributions of avalanche dynamics. *Sci. Rep.* **10**, 626 (2020).
26. C. Collettini, G. Di Stefano, B. Carpenter, P. Scarlato, T. Tesei, S. Mollo, F. Trippetta, C. Marone, G. Romeo, L. Chiaraluce, A novel and versatile apparatus for brittle rock deformation. *Int. J. Rock Mech. Min. Sci.* **66**, 114–123 (2014).
27. M. M. Scuderi, C. Marone, E. Tinti, G. Di Stefano, C. Collettini, Precursory changes in seismic velocity for the spectrum of earthquake failure modes. *Nat. Geosci.* **9**, 695–700 (2016).
28. M. A. Sutton, J. J. Orteu, H. Schreier, *Image correlation for shape, motion and deformation measurements: basic concepts, theory and applications* (Springer Science &

Business Media, 2009).
29. P. Bhattacharya, A. M. Rubin, E. Bayart, H. M. Savage, C. Marone, Critical evaluation of state evolution laws in rate and state friction: Fitting large velocity steps in simulated fault gouge with time‐, slip‐, and stress‐dependent constitutive laws. *J. Geophys. Res. Solid Earth*. **120**, 6365–6385 (2015).
30. F. Yamashita, E. Fukuyama, K. Mizoguchi, S. Takizawa, S. Xu, H. Kawakata, Scale dependence of rock friction at high work rate. *Nature*. **528**, 254–257 (2015).
31. L. Buijze, Y. Guo, A. R. Niemeijer, S. Ma, C. J. Spiers, Nucleation of stick‐slip instability within a large‐scale experimental fault: Effects of stress heterogeneities due to loading and gouge layer compaction. *J. Geophys. Res. Solid Earth*,. **125**, e2019JB018429 (2020).
32. S. M. Rubinstein, G. Cohen, J. Fineberg, Contact area measurements reveal loading-history dependence of static friction. *Phys. Rev. Lett.* **96**, 256103 (2006).
33. L. B. Hunfeld, A. R. Niemeijer, C. J. Spiers, Frictional Properties of Simulated Fault Gouges from the Seismogenic Groningen Gas Field Under In Situ P–T -Chemical Conditions. *J. Geophys. Res. Solid Earth*. **122**, 8969–8989 (2017).

Acknowledgments

We thank Marco Scuderi of Sapienza University, Rome for performing the experiments on the 5 cm scale.

Funding:

Nederlandse Aardolie Maatschappij (NAM) contract UI:49294

European Research Council (ERC) starting grant SEISMIC 335915 (ARN)

Netherlands Organization for Scientific Research (NWO) through VIDI grant 854.12.011. (ARN)

Author contributions:

Conceptualization: ARN, CJS, EF, YJ, FY, SX

Methodology: YJ, ARN, DHB, EF, FY, SX

Data acquisition, analysis, interpretation: YJ, ARN, DDH, FY, SX, LBH, RPJP, EF, CJS

Visualization: YJ

Funding acquisition: CJS, ARN

Project administration: CJS, ARN

Supervision: CJS, ARN

Writing – original draft: YJ, ARN, CJS

Writing – review & editing: YJ, CJS, ARN, EF, FY, SX

Competing interests: Authors declare that they have no competing interests.

Data and materials availability: Data will be made available via the EPOS-NL repository at Utrecht University. DOI follows.

Figures and Tables

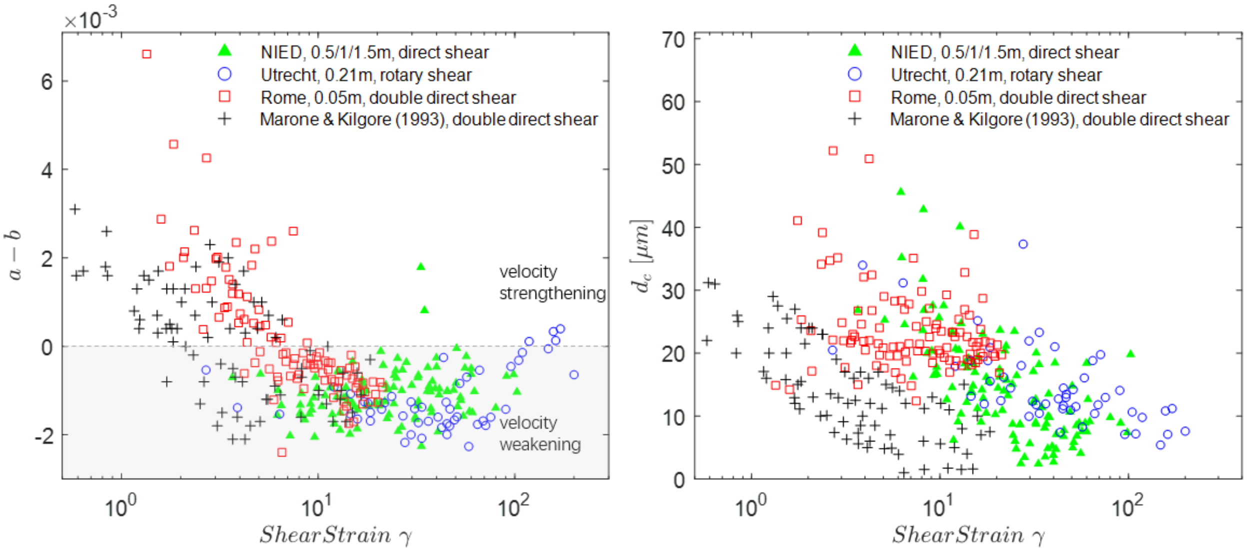

Fig. 1. RSF parameters vs. shear strain. The friction properties obtained in gouge friction experiments performed at different length scales with initial gouge thicknesses of 1-5 mm. Left: (*a*-*b*), Right: d_c. Shear strain represents slip distance normalized to instantaneous gouge thickness.

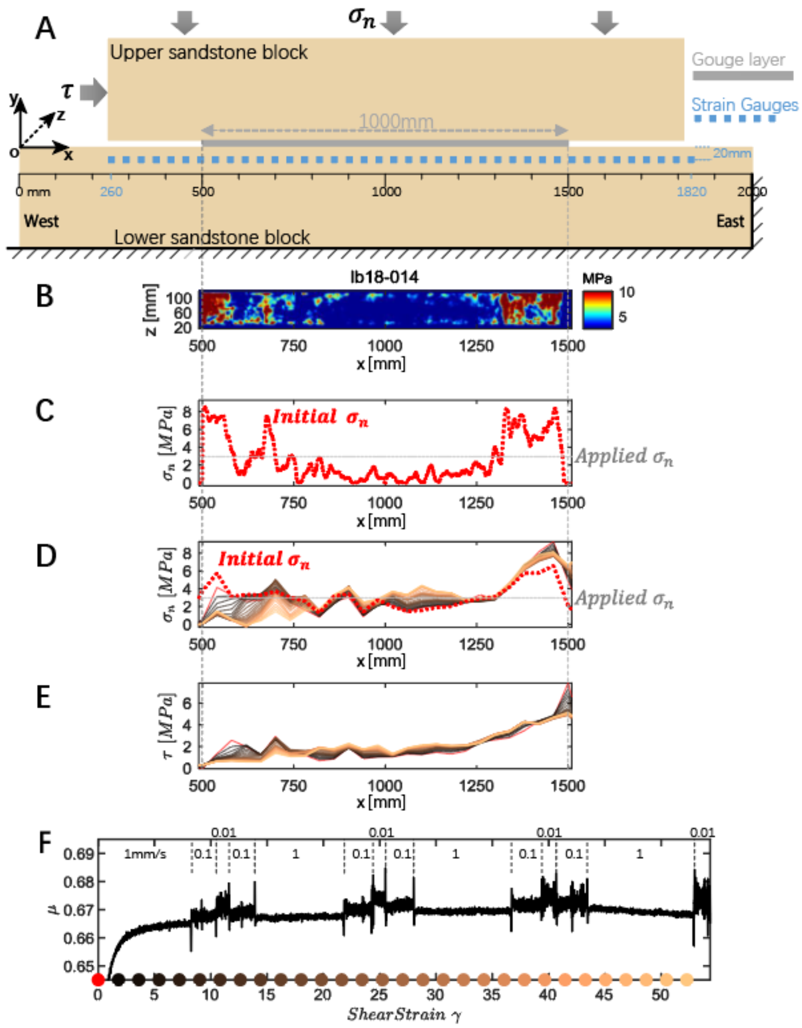

Fig. 2. Experimental configuration and data for experiment LB18-14 (3 MPa normal stress, 3 mm gouge thickness, 1 m gouge length). (**A**) Large-scale direct shear set-up at NIED, see Supplement. (**B**) Initial normal stress on gouge layer (0.1 m by 1 m) obtained using pressure-sensitive-sheet. (**C**) Average normal stress vs. position along the fault length, calculated from B. (**D**), (**E**) Normal and shear stress distribution and evolution with time along the fault, derived from strain gauges. Dotted red curve in (D) is the initial normal stress distribution measured before shearing (γ=0). (**F**) Concurrently measured macroscopic friction coefficient against shear strain γ. Note that the applied or "load point" velocity was cycled between 1.0, 0.1 and 0.01 mm/s. Colored dots along the γ-axis correspond to the curve colors in (D)-(E).

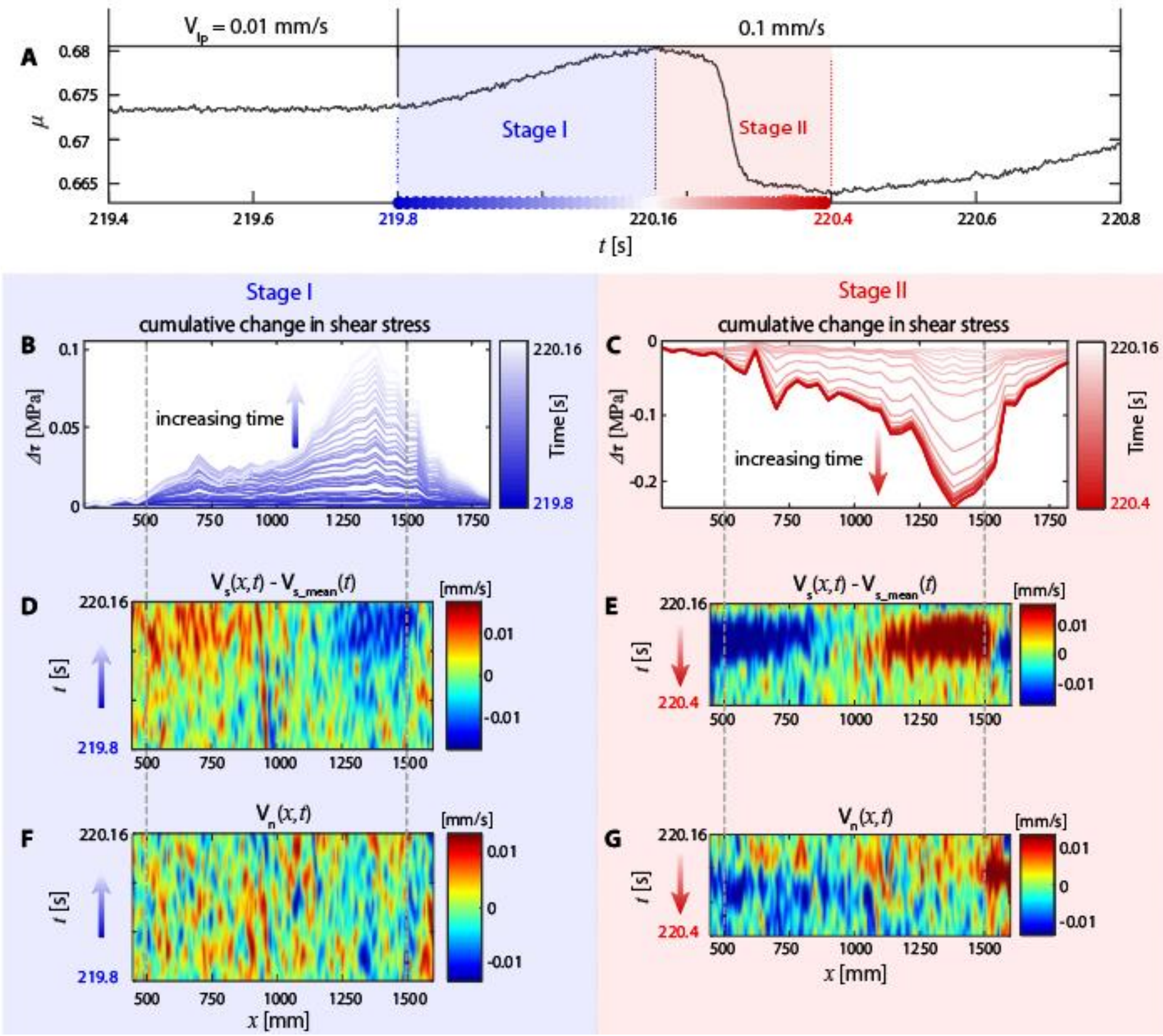

Fig. 3. Spatio-temporal evolution during and after a velocity step. Spatio-temporal evolution of shear stress and across-fault velocity components in experiment LB18-23, during and after a velocity-step (t= 219.8s – 220.4s) from 0.01 to 0.1 mm/s. (**A**) Macroscopic friction coefficient vs. time (timescales as in B-C). (**B**)-(**C**) Shear stress evolution (change $\Delta\tau$) measured over the time interval sampled (blue/red bars in A-C). (**D**)-(**E**) Departure from the mean shear velocity determined at each time instant, expressed by subtracting the average relative slip rate along the fault $V_{s\_mean}(t)$ from the relative slip velocity $V_s(x, t)$ measured across the gouge at each location along its length. Shear stresses and velocities are measured right lateral positive. (**F**)-(**G**) Normal component of relative velocity ($V_n(x, t)$) of the upper block to the lower block (dilation positive). Dashed vertical lines mark gouge layer extent.

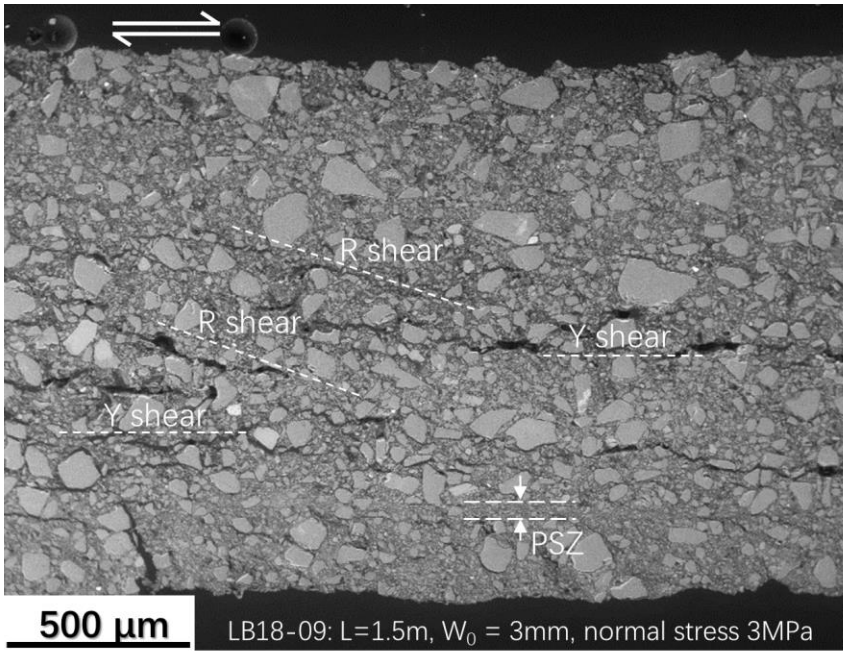

Fig. 4. Typical gouge microstructure in present experiments (Scanning Electron Microscope image in backscatter electron mode, sample LB18-09 length 1.5m). Macroscale fault slip ($\rightleftharpoons$) is accommodated via microscale shear bands (R, Y and principal Y slip zone PSZ) with mm-scale spacing.